International Journal of Nanoelectronics and Materials
IJNeaM
ISSN 198-5761 | E-ISSN 2232-1535

In Press, Accepted Manuscript – Note to user

Revisiting the Optoelectronic Properties of Graphene: A DFT Approach

A. L Olatomiwa[a,b]+, Alaa Kamal Yousif Dafhalla[c], A.Wesam Al-Mufti[d], Z.A. Arsat[e], Tijjani Adam[a,b,h] + Abdullah Chik[f], Subash C.B. Gopinath[a,f,h], M.N.A Uda[e], M.N. Afnan Uda[g], Uda Hashim[a]

[a]*Institute of Nano Electronic Engineering, Universiti Malaysia Perlis, 01000, Perlis, Malaysia*
[b]*Faculty of Electronic Engineering and Technology, Universiti Malaysia Perlis, 02600 Arau, Perlis, Malaysia*
[c]*Department of Computer Engineering, College of Computer Science and engineering, University of Ha'il, KSA*
[d]*Department of medical physics, College of Science, Al-Karkh University of science. Baghdad. Iraq*
[e]*Faculty of Mechanical Engineering & Technology, Universiti Malaysia Perlis, 02600 Arau, Perlis.*
[f]*Materials Department, Faculty of Chemical Engineering & Technology, Universiti Malaysia Perlis (UniMAP), UniMAP School Complex, Taman Muhibah, Jejawi 02600, Perlis, Malaysia*
[g]*Faculty of Engineering, Universiti Malaysia Sabah, 88400 Kota kinabalu , Sabah ,Malaysia*
[h]*Micro System Technology, Centre of Excellence (CoE), Universiti Malaysia Perlis (UniMAP), Pauh Campus, 02600 Arau, Perlis, Malaysia.*
∗Corresponding authors. Tel.: +234-70-3650-8896, +601112515077; e-mail: olatomiwa@studentmail.unimap.edu.my and tijjani@unimap.edu.my.

Received 24 February 2023, Revised 2 June 2023, Accepted 25 August 2023

ABSTRACT

The understanding of the atomic behaviour of pure graphene is crucial in manipulating its properties for achieving optoelectronics with high absorption index and efficiencies. However, previous research which employed the DFT emphasized its zero-band gap nature and not its unique optical properties. Therefore, this study employed the ab initio calculations to revisit the electronic, magnetic, and optical properties of pristine graphene using the WIEN2K code. The results reveal that the PBE-GGA valence and conduction bands were found to cross at -0.7 eV. Our Calculations demonstrated that the absorption coefficient of graphene has the strongest light penetration in the parallel direction. Furthermore, our results not only present the best propagation of light in pure graphene but also reveal that the linear relationship between the formation of the free electron carriers and the energy absorption is responsible for the high optical conductivity observed in pure graphene, as indicated by the peaks. Lastly, the metallic properties of graphene are reflected by the variation in spin up and down that appears, as evidenced by the total and partial densities of states, and the large refractive index attributed to its high electron mobility confirms its metallic nature.

Keywords: High electron mobilities; linear dispersion; large refractive index; and parallel light penetration.

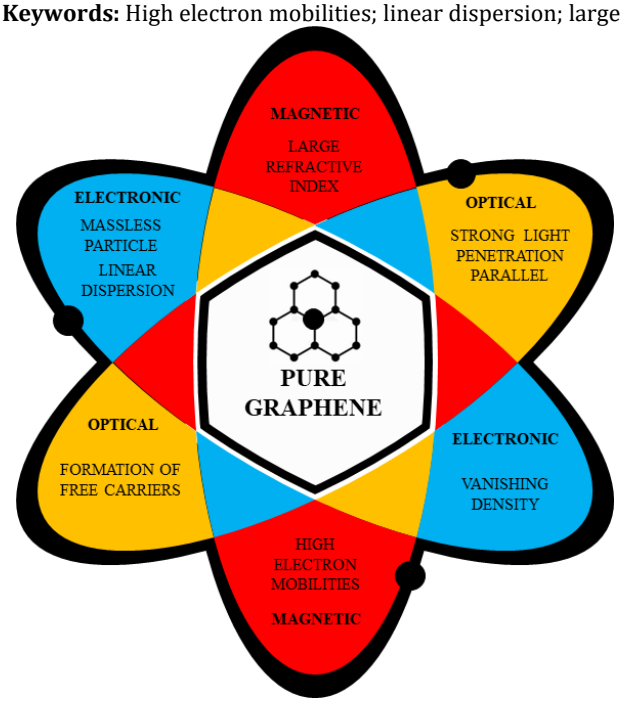

1. INTRODUCTION

The discovery of graphene was achieved in 2004 by professors at the University of Manchester, Andre Geim and Kostya Novoselov, who mechanically exfoliated high pyrolytic graphite to create a monolayer of graphene on a sticky tape Highly oriented pyrolytic graphite (HOPG). It is an essential element of graphite, carbon nanotubes, and other allotropes of carbon, including fullerenes (0D), carbon nanotubes, and (3D) [1][2][3]. As a result of their ground-breaking discoveries and contributions to science, they were bestowed the 2010 Nobel Prize [4][5][6]. A large group of 2D nanomaterials, including silicene, hexagonal boron nitride (h-BN), transition-metal dichalcogenides (TMDs), and phosphorene, have emerged because of the emergence of this one-atom-thick layer of graphite with sp2 hybridized carbon atoms arranged in a hexagonal honeycomb lattice. These materials exhibit a wide range of properties, from the weakest to the strongest and from the best insulating to the most conducting materials[7][8][9].

However, Pristine graphene, a gapless 2D nanomaterial with high intrinsic carrier mobility (200,000 $cm^2V^{-1}S^{-1}$), large surface area (2630 m^2g^{-1}), high Young's modulus (~1.0 TPa), thermal conductivity (~5000 $Wm^{-1}k^{-1}$), and good electrical conductivity distinguishes itself with its remarkable properties. Its optical property includes excellent optical transmittance (~97.7%) and it can resist a current density of 108 A/cm^2 making it an ideal material for widespread applications in optoelectronics [10][11][12][13]. Furthermore, the zero-mass asymmetric Dirac fermion behaviour allows the exploration of a variety of fascinating behaviour that is consistent with the relativistic regime's predictions [14][15]. However, the band degeneracy at the Dirac points in the hexagonal Brillouin zones limits its application in electronic devices due to its low on and off current. Despite this, the inherent carrier mobility in graphene has made it a leading alternative to silicon material in Nano-electronics with the monolayer graphene exhibiting an optical absorption of 2.3% throughout a broad spectrum from Tetra-hertz to visible light frequencies. Therefore, positioning graphene for applications in high-speed photodetectors and solar cell devices [16][17][18]. Moreover, despite the ability of graphene's ability to absorb 2.3 % of photons in the electromagnetic spectrum given its atomic size, the efficiency of photovoltaics and sensing devices are significantly limited [17].

Thus, it is very important to improve its application in electronic devices and its optical performance for efficient light absorption in the electromagnetic spectrum. Several studies have attempted to model its electronic properties through substitutional doping to enhance its properties [19]. However, despite the considerable success, most of the dopants employed in literature, the limitations of band gap engineering, structural defects, and stability persists[20]. This is associated to an insufficient understanding of the atomic behaviour of pure graphene, nature of the dopants and substitutional doping sites. Thus, revisiting the optoelectronic properties of pure graphene via the DFT approach is crucial to unlocking its ubiquitous potentials [17][20][21].

Therefore, to achieve efficient light absorption for graphene-based optoelectronics the understanding of its electronic, optical, and magnetic properties atomically is key to manipulating its excellent intrinsic properties. Different studies have examined the properties of pure graphene but based on our findings, no report has explored graphene's electronic structure, and optical, and magnetic properties using DFT calculations. Therefore, we have not only carried out research that covers all the above-mentioned properties, but our results will enhance the accuracy beyond existing studies. We demonstrate how the unique electronic, optical, and metallic properties can be exploited in designing photovoltaics and sensing devices with very high absorption index and efficiencies.

2.0 COMPUTATIONAL METHODS

A density functional theory study with the WIEN2K package's full potential linearly augmented plane wave (FP-LAPW) technique was used to determine the electronic structure, magnetic, and optical properties of pure graphene [22]. The augmented plane wave plus local orbitals (APW+lo) technique, which considers all electrons (core and valence) in a self-consistent way, is employed by the WIEN2k software to solve the Kohn-Sham equations of density functional theory. To prevent contact between the atoms in the atomic configuration of graphene considered, a large vacuum of 18 Å was selected for this work. The minimum energy was calculated employing the Generalized Gradient Approximation with the Perdew-Burke-Ernzerhof (GGA-PBE) functional potential, which effectively considers Å exchange-correlation (XC) interactions [19].

To calculate self-consistent fields, the first Brillouin zone (BZ) was sampled using a Monkhorst-Pack with a k-point of 1000, RMT*Kmax = 7.0, and Gmax = 12.0. Convergence of energy and charge was investigated, with convergence limits set at 0.0001 for energy and 0.001 for a charge, to be attained iteratively using the self-consistent field (SCF) approximation. Additionally, very dense data was employed to calculate additional properties: 10000 k points were employed to calculate the density of state and optical parameters. Because the optical spectrum is dependent on incoming electromagnetic waves, it was computed using the real $\varepsilon_1(\omega)$ and imaginary components $\varepsilon_2(\omega)$ of the dielectric function. The relationship employed to represent the dielectric function is expressed in Eq. (1):

$$\varepsilon(\omega) = \varepsilon_1(\omega) + i\varepsilon_2(\omega) \quad (1)$$

Therefore, ε_2 in the limit of long wavelength is written as follows in Eq. (2):

$$\varepsilon_2(q \longrightarrow 0, \omega) = \frac{2e^2\pi}{V\varepsilon_0} \sum_{VB,CB,k} \left|\langle \psi_k^{cB} | \vec{a} \cdot \vec{b} | \psi_K^{VB} \rangle\right|^2 \delta(\mathrm{E}_k^{CB} - \mathrm{E}_K^{VB} - \omega) \quad (2)$$

Where ε_0, and V depicts the permittivity of free space, and volume of the supercell of the electromagnetic radiation, respectively. The valence and conduction bands are represented by V. B and C. B. Therefore, $\vec{a}$ and $\vec{b}$ depicts the incident electromagnetic field's polarization vector and position, respectively [23], [24].

$$\varepsilon_1 = 1 + \frac{2}{\pi} P_0 \int_0^\infty \frac{\omega' \varepsilon_2(\omega')}{\omega'^2 - \omega^2} d\omega' \quad (3)$$

Where P_0 = the principal value and $\omega =$ frequency, respectively as expressed in Eq. (3).

Both $\varepsilon_1 \, and \, \varepsilon_2$ are independent components related to the two polarizations of the electric field in connection to the system considered [25]. The $\varepsilon_\parallel \, and \, \varepsilon_\perp$ which denote the parallel and perpendicular directions are the polarizations considered in this study. The complex refractive index (n_i) is expressed in Eq. (4). with both $n\,(\omega) and\, k\,(\omega)$ indicate the both the real and imaginary parts related to the optical constant in Eq. (5) and (6), respectively. The refractive index is represented by $n\,(\omega)$ while the extinction coefficient is indicated by $k\,(\omega)$ [26].

$$n_i(\omega) = n(\omega) + ik\,(\omega) \quad (4)$$

$$n\,(\omega) = \left[\frac{\sqrt{\varepsilon_1^2 + \varepsilon_2^2}}{2} + \frac{\varepsilon_1}{2}\right]^{\frac{1}{2}} \quad (5)$$

$$k\,(\omega) = \left[\frac{\sqrt{\varepsilon_1^2 + \varepsilon_2^2}}{2} - \frac{\varepsilon_1}{2}\right]^{\frac{1}{2}} \quad (6)$$

The reflectivity (R) of the system written in Eq. (7) is determined by the polarized field incident normal to the material.

$$R\,(\omega) = \left(\frac{1 - \sqrt{\varepsilon(\omega)}}{1 + \sqrt{\varepsilon(\omega)}}\right)^2 \quad (7)$$

The coefficient of the absorption spectra $(\alpha(\omega))$ in Eq. (8) is expressed as follows:

$$\alpha(\omega) = \frac{2k\omega}{v} \quad (8)$$

Where v represents the velocity of light in a vacuum.

3. DISCUSSION AND RESULTS

3.1. Structural properties

Fig. 1, reveals the optimized 2×2 supercell of pure graphene. After optimization, the relaxed lattice parameters of pure graphene were found to be $a = b = 2.46$ Å with $\alpha = \beta = 90° and\, \gamma = 120°$ and a $C - C$ bond length of 1.42 Å. The volume optimization plot is displayed in Fig. 2. The calculated covalent σ bond formed by Sp^2 hybridization observed in pure graphene is stronger than the $C - C$ bonds observed in diamond with Sp^3 hybridization, and this value is consistent with the previous report [27].

A vacuum space in the z-axis of 18.00 Å was selected to prevent interlayer interactions between the layers of the pristine graphene and the space group of 194 $P6_3/mmc$, and a hexagonal structure was considered. The value of the optimized lattice parameter is consistent with values reported in the literature [28]–[30].

3.2 Electronic Properties

The GGA-PBE was employed to determine the electronic band structure and density of states (DOS) for the pure graphene 2x2 supercell [31]. The calculated electronic band structure is displayed in Fig. 3, along the high symmetry axis (Γ – M –K– Γ) and the first Brillouin zone. Due to the linear dispersion relation at E = 0, the valence and conduction band in both exchange-correlation functionals overlap at the Dirac sites with zero band gaps, showing the fermions at this location behave as massless particles as displayed in Table 1. The linear dispersion (E) relation of graphene is expressed in Eq. (9) [32], [33].

$$\mathrm{E} = \frac{hkV_F}{2} \quad (9)$$

Where h= Planck's constant, k = Dirac Point, and $V_F \;\; (Femi\; velocity) = c/300$.

The valence and conduction bands cross at -0.7eV, indicating Pristine graphene behaves like a semimetal with high electrical conductivity. As a result, the obtained results verifies that pure graphene has an intrinsic metallic nature (unmatched electrical conductivity) because its electronic state creates ideal Dirac cones at energies close to the degeneracy point confirming the previously reported theoretical and experimental findings which validate the accuracy of our findings.[34]–[36].

Fig. 4(a-b) illustrates the obtained results for the DOS of Pure graphene. The density of state provides a baseline knowledge concerning electrons of transfer from the valence to conduction bands while also determining electronic orbital property across an energy range in the band structure [37]. The DOS for graphene which defines it as a metal with a zero-band gap was deduced in Eq. (10) [38]:

$$D\,(E) = \frac{2\pi|E|}{h^2 v^2} \quad (10)$$

This vanishes as $\mathrm{E} \rightarrow 0$.

Fig. 4 (a-c) illustrates the total and partial density of states of pure graphene with all the important states ranging from -7 to 17eV. Both the total and partial density of the state shows that pristine graphene has a zero-band gap as $\mathrm{E} \longrightarrow 0$ at the Fermi level as revealed in Fig. 3 [39]. This shows the reliability of our calculation which is also consistent with different reports in the literature [40]–[43].

In Fig. 4 (a-b) the main peak appears at 8.85 eV at a height of 2 in the conduction band. However, more peaks appear in the conduction band than in the valence band and the peaks in the conduction band appear at 2 eV, 11.2 eV, 12.8 eV, and 17 eV at a height of 0.72, 1.2, 1.4, and 1.3, respectively while the peaks at the valence band appear at -7 and -2 eV at a maximum of 1.36 and 0.7 respectively. The band structure indicated that pristine graphene is a massless particle that exhibits linear dispersion throughout the region [44].

The partial density of states plots in Fig. 4(c) emphasizes that the p orbital has the greatest contribution in pristine graphene. The positions of the peaks observed in the total DOS agree with the partial density of states. Fig. 4 (c) curves also indicate that the two electronic bands in graphene are a P_Z character and contributes more based on the peaks and intersecting at the Fermi level with adsorption for low energy [31], [45], [46].

3.3 Magnetic Moment

The calculated magnetic moments for pure graphene are indicated in Table 2. based on the contribution of the individual C-C atoms in the configuration highlighting the interstitial and the spin (total) magnetic moment. The difference observed in the spin up and down as revealed in the total and partial density of states indicates the metallic properties of graphene. The symmetry of both spin channels in the plots for the DOS and the intrinsic non-magnetic behaviour of graphene was further confirmed by the inconsequential values of the magnetic moments of the pure graphene system [47], [48].

3.4 Optical Properties

3.4.1 Dielectric function

Fig. 5(a-b) shows the real, ε_1, and imaginary, ε_2 halves of the dielectrics for pure graphene in parallel $\varepsilon_{\parallel}$ and $\varepsilon_{\perp}$ polarization of light in the electromagnetic spectrum. The major optical characteristics of the crystal are determined by a variety of spectrum data represented by the dielectric function, including the configuration of the solid energy band [31], [44]. The real section of pure graphene's dielectrics is displayed in Fig. 5a.

The static dielectric constant in the $\varepsilon_{\parallel}$ polarization appears at 33 and 1.8 in the $\varepsilon_{\perp}$ electromagnetic polarization (i.e., real dielectric = 0 eV. Graphene's absorption spectra are determined by the imaginary half of the dielectric function. [49], [50]. The primary peaks of the imaginary part of graphene in the $\varepsilon_{\parallel}$ polarization is at 4.2 eV and 13.4 eV, respectively, and is consistent with earlier results in the literature [33], [36], [49]. These two peaks arise from $\pi \longrightarrow \sigma^*$ and $\sigma \longrightarrow \pi^*$ inter-bands transitions in the $\varepsilon_{\parallel}$ propagation of light. However, a single peak appears at 10.6 eV in the $\varepsilon_{\perp}$ polarization of the EM wave. These results are consistent with existing reports in the literature [50], [51].

3.4.2 Absorption Coefficient

The absorption coefficient of graphene is a function of incident light in $\varepsilon_{\parallel}$ and $\varepsilon_{\perp}$ polarization of light is revealed in Fig. 6. Two prominent peaks with optical frequencies appear in the $\varepsilon_{\parallel}$ polarization at 4.2 and 13.8 eV. In the same direction, it is found that the second peak has a more prominent intensity than the first peak. Additionally, a prolonged optical frequency peak measuring 12.2 eV at a maximum of 16.5 in the $\varepsilon_{\perp}$ electromagnetic polarization.

However, a coefficient value of roughly 0.1 was found in the range of visible light in the $\varepsilon_{\parallel}$ polarization from 8.2 to 10 eV. According to Ref. [15], the absorption coefficient determines the amount of photon energy at a specified wavelength that travels through a medium before being absorbed by it. Thin films made of substances with high absorption coefficients may allow the passage of optical wavelengths with low absorption coefficients. These peaks are caused by two fundamental transitions between graphene's electronic states while the remaining peaks represent the transition of carbon-carbon from the Fermi level-closed state in the region for carbon interaction, the largest peak represents the shift from an occupied to an unoccupied state [52], [53].

In this study, it is found that the $\varepsilon_{\parallel}$ polarization has stronger light penetration than the $\varepsilon_{\perp}$ electromagnetic polarization with its very high absorption coefficient in the ultraviolet and visible ranges as reported in several studies [49], [54], [55]. According to Ref. [56], the behaviour of the optical absorption in the $\varepsilon_{\parallel}$ electromagnetic propagation suggests that it can radically alter the absorption characteristics of graphene by rearranging the atoms in this direction. As a result, graphene will enhance its ability to absorb light in the visible light spectrum. Therefore, this study concludes that based on the results in the $\varepsilon_{\parallel}$ electromagnetic polarization the graphene's optical properties are strongly dependent on the parallel region.

3.4.3 Optical Reflectivity

The reflectivity of pure graphene is revealed in Fig. 7 as a function of incident light and wavelength, respectively, in $\varepsilon_{\parallel}$ and $\varepsilon_{\perp}$ propagation of light. The optical reflectivity R (ω) is the percentage of light that is reflected at an interface. The ratio of the amplitudes of the incident and reflected waves is known as the reflection spectrum. We discovered that pristine graphene's reflectance rises with energy in the $\varepsilon_{\parallel}$ electromagnetic polarization at energies below 8 eV.

A large peak with an intensity of 0.5 appears at 4.2 eV in the same direction, where reflectivity also rises as a function of energy for energies greater than 9 eV. However, we observe that in the parallel polarization of the incident light at the interval of 8.6 to 10 eV, the peak at the visible range in the EM spectrum vanishes. In the $\varepsilon_{\perp}$ electromagnetic polarization, a maximum reflectivity of 12.2 eV appears with an intensity of 0.31, and from the interval of 8.2 to 13.2 eV, and this has a higher reflectivity than the $\varepsilon_{\parallel}$ electromagnetic polarization of EM wave.

Therefore, Fig. 7 reveals that in the $\varepsilon_{\parallel}$ polarization of photon energy concerning the plane of the pristine graphene, a negligible reflectivity at higher energy is expected, which indicates that there would be a higher transition in this direction which confirms existing results [36], [57], [58]. Therefore, an unchanged reflectivity is expected in the range of 8.6 eV to 10 eV region for pristine graphene [49], [55], [59].

3.4.4 Energy loss function (EELS)

Plasmon's, surface Plasmon's, and inter-band transitions are all collective excitations that are measured by the energy loss function, which is expressed below [60] The process by which some energy is lost because of the electrons' rapid motion as electromagnetic light passes through a substance is represented by the function L(ω).

It can be deduced from $L\ (\omega) =\ \mathrm{IM}\left((q\ \rightarrow 0, \omega) - \frac{1}{\varepsilon}\right)$ in Eq. (11) with an increase in size as ε_1 vanishes and $\varepsilon_2\ < 1$ at the plasma frequency [31], [55].

$$\mathrm{L}\ (\omega) =\ \frac{\varepsilon_2}{\varepsilon_1^2 +\ \varepsilon_2^2} \qquad (11)$$

The results of EELS could reveal details about elastically scattered and non-scattered electrons in addition to the type and atomic number that the beam may strike [31]. A major peak appears at 7.4 eV with an intensity of 2.4 and another peak appears between 11.2 eV to 13.4 eV with an intensity that lies between 0.12 and 0.3 in the $\varepsilon_{\parallel}$ electromagnetic polarization.

The major peak in the $\varepsilon_{\perp}$ electromagnetic polarization appears at 12.8 eV with peak intensities of 0.60. In the electromagnetic polarization, 0% energy loss was recorded in the ultraviolet and visible light range, which indicates that there is no apparent scattering in this direction. However, the $\varepsilon_{\parallel}$ polarization has a coefficient value of approximately 0.1 in the interval of 9.2 eV to 11.2 eV and the $\varepsilon_{\perp}$ polarization has a higher electron energy loss at higher energies in the interval of 10.3 eV to 13.2 eV. The primary peak corresponds to the change from an occupied (π) to an unoccupied state (π*), and the remaining peaks correspond to the change of carbon-carbon from the region near the Fermi level for the carbon interaction.

3.4.5 Complex Refractive Index

This is the product of the normal refractive index $n\ (\omega)$ and the extinction coefficient $\kappa(\omega)$, as shown by the relation [31]. In Fig. 9(a-b), $n\ (\omega)$ and $\kappa(\omega)$ of the complex refractive index in the parallel and perpendicular polarization are determined by equations (5) and (6). The refractive index of pristine graphene in the $\varepsilon_{\parallel}$ polarization has two major peaks at 4.0 and 11.4 eV and a corresponding peak at 2.55 and 1.8, while a peak at 10.4 eV appears with an intensity of 2.4 and falls at this height in the $\varepsilon_{\perp}$ polarization, which corresponds to the peak at 10.4 eV in the same direction as the absorption coefficient, validating the accuracy of our results.

The peaks observed in the spectrum indicate a maximum $n(\omega)$ value at that orange. These agree with previous studies by Olaniyan *et al*. [48] and Rani et al [45]. According to Fig. 9b, the decrease in the most extreme peak of $\kappa(\omega)$ is due to quantum confinement, which is discussed in more detail in our next paper. Moreover, a vanishing coefficient value of approximately 0.1 was observed in the interval of 8.2 to 10 eV in the parallel polarization of the optical reflectivity in the $\varepsilon_{\parallel}$ polarization.

Moreover, in the $\varepsilon_{\perp}$ polarization a peak is found at 13.8 eV with an intensity of 1.7. The real part explains light refraction caused by changes in light speed in graphene, whereas the imaginary part (extinction coefficient) indicates light absorption or attenuation in a solid [61]. As a result, the large refractive index value in metallic nature compounds can be attributed to electron-free mobility. Its metallic nature has higher refractive index values, making it a good choice for photovoltaic or optoelectronic applications.

3.4.6 Optical Conductivity

The gapless behavior in the band structure of graphene makes it a good electrical conductor [36]. The frequency of a compound, which affects its optical conductivity, is an important parameter in the analysis of the electronic states of materials. Free carriers are formed because of incident absorption energy, as shown by the optical conductivity (σ). The expression in Eq. (12) shows the conductivity (σ_0) of graphene:

$$\sigma_0 = \frac{g_v g_s\, e^2}{\pi h W} \qquad (12)$$

Where $W = n_i = \langle u_i^2 \rangle \frac{E_F}{h^2 V^2}$

The expressions above reveal that by neglecting the potential dependency of the scattering intensity on E_F or n_s, graphene's conductivity is distinct from the Fermi energy and the carrier concentration. As a result, graphene ought to be viewed as a metal rather than a semiconductor [38].

In Fig. 10(a-b), the calculated real and imaginary optical conductivity of pure graphene in $\varepsilon_{\parallel}$ and $\varepsilon_{\perp}$ polarization of electromagnetic waves; it also shows that graphene is a gapless material because the conductivity begins at 0 eV in both polarization of the electromagnetic wave. For the real optical conductivity in the $\varepsilon_{\parallel}$ propagation, two peaks are found at 4.2 and 13.2 eV with an intensity of 5.2 and 6.25, which is like the absorption coefficient in the $\varepsilon_{\parallel}$ polarization as displayed in Table 3.

In the $\varepsilon_{\perp}$ polarization a peak arises at 10.8 eV at an intensity of 6.4. A peak was observed in the $\varepsilon_{\parallel}$ polarization at 4.2 eV at an intensity of 1.92. However, both $\varepsilon_{\parallel}$ and $\varepsilon_{\perp}$ polarization falls at 11.4 eV and 10.2 eV which rises to a height of 1.7 and 5.2 at 13.8 eV and 12.2 eV. The very high optical conductivities observed in both the real and imaginary parts reveal the metallic nature of pristine graphene as shown in Table 4. These findings agree with reports in the literature [62].

4. CONCLUSION

Pure graphene has shown wonderful behaviour, especially in the electronics field. It can be engineered with optimized atomic content or by adding controlled impurities, making it a particularly promising electronic material. The focus of this study is to provide a comprehensive understanding of the atomic behaviour of pure graphene. In this research, the electronic, magnetic, and optical properties and bonding characteristics of pure graphene were examined using first principles (DFT) with the FP-

LAPW technique. The calculated results show that the graphene structural dimension was found to be a = b = 2.46 Å and c = 18.00 Å, α = β = 90° and γ = 120°. Furthermore, it was found that the best propagation of light in pure graphene lies in the parallel direction, and the linear relationship between the formation of the free electron carriers and the energy absorption is responsible for the high optical conductivity (σ) observed in pure graphene. Besides, the metallic properties of graphene are reflected by the variation in spin up and down that appears, as evidenced by the total and partial densities of states, and the large refractive index attributed to its high electron mobility confirms its metallic nature. Lastly, despite the challenge faced in manipulating properties of graphene. Our results demonstrate that the DFT approach has the potential to provide valuable insights into the properties of graphene and explore its prospects for optoelectronic devices.

ACKNOWLEDGMENTS

A.L Olatomiwa acknowledges Malaysia International Scholarship (MIS) for funding his Master of Science (MSc) in Nanomaterial Engineering at the Institute of Nano Electronic Engineering, Universiti Malaysia Perlis, Malaysia.

REFERENCES

[1] M. Yi and Z. Shen, "A review on mechanical exfoliation for the scalable production of graphene," *J Mater Chem A Mater*, vol. 3, no. 22, pp. 11700–11715, 2015, doi: 10.1039/c5ta00252d.

[2] L. Chen, Y. Hernandez, X. Feng, and K. Müllen, "From nanographene and graphene nanoribbons to graphene sheets: Chemical synthesis," *Angewandte Chemie - International Edition*, vol. 51, no. 31, pp. 7640–7654, 2012, doi: 10.1002/anie.201201084.

[3] S. Zhang, J. Zhou, Q. Wang, X. Chen, Y. Kawazoe, and P. Jena, "Penta-graphene: A new carbon allotrope," *Proc Natl Acad Sci U S A*, vol. 112, no. 8, pp. 2372–2377, 2015, doi: 10.1073/pnas.1416591112.

[4] D. Ion-Ebrasu *et al.*, "3-D graphene growth by chemical vapor deposition (CVD) for energy applications," *Smart Energy and Sustainable Environment*, vol. 23, no. 1, pp. 13–20, 2020, doi: 10.46390/j.smensuen.23120.77.

[5] A. Jilani *et al.*, "Graphene and its derivatives: synthesis, modifications, and applications in wastewater treatment," *Environ Chem Lett*, vol. 16, pp. 1301–1323, 2018, doi: 10.1007/s10311-018-0755-2.

[6] B. R. Sharma, A. Manjanath, and A. K. Singh, "Pentahexoctite: A new two-dimensional allotrope of carbon," *Sci Rep*, vol. 4, pp. 4–9, 2014, doi: 10.1038/srep07164.

[7] S. Hassan Mir, V. Kumar Yadav, and J. Kumar Singh, "Recent Advances in the Carrier Mobility of Two-Dimensional Materials: A Theoretical Perspective," 2020, doi: 10.1021/acsomega.0c01676.

[8] K. Cho, J. Yang, and Y. Lu, "Phosphorene: An emerging 2D material," *J Mater Res*, vol. 32, no. 15, pp. 2839–2847, 2017, doi: 10.1557/jmr.2017.71.

[9] P. Ajayan, P. Kim, and K. Banerjee, "Two-dimensional van der Waals materials," *Phys Today*, vol. 69, no. 9, pp. 38–44, 2016, doi: 10.1063/PT.3.3297.

[10] M. Lobet, B. Majerus, L. Henrard, and P. Lambin, "Perfect electromagnetic absorption using graphene and epsilon-near-zero metamaterials," *Phys Rev B*, vol. 93, no. 23, Jun. 2016, doi: 10.1103/PhysRevB.93.235424.

[11] V. Georgakilas, J. A. Perman, J. Tucek, and R. Zboril, "Broad Family of Carbon Nanoallotropes: Classification, Chemistry, and Applications of Fullerenes, Carbon Dots, Nanotubes, Graphene, Nanodiamonds, and Combined Superstructures," *Chem Rev*, vol. 115, no. 11, pp. 4744–4822, 2015, doi: 10.1021/cr500304f.

[12] Z. Zhang, J. Zhang, N. Chen, and L. Qu, "Graphene quantum dots: An emerging material for energy-related applications and beyond," *Energy Environ Sci*, vol. 5, no. 10, pp. 8869–8890, Oct. 2012, doi: 10.1039/c2ee22982j.

[13] A. Adetayo and D. Runsewe, "Synthesis and Fabrication of Graphene and Graphene Oxide: A Review," *Open Journal of Composite Materials*, vol. 09, no. 02, pp. 207–229, 2019, doi: 10.4236/ojcm.2019.92012.

[14] C. H. Park, L. Yang, Y. W. Son, M. L. Cohen, and S. G. Louie, "Anisotropic behaviours of massless Dirac fermions in graphene under periodic potentials0," *Nat Phys*, vol. 4, no. 3, pp. 213–217, 2008, doi: 10.1038/nphys890.

[15] D. S. L. Abergel, V. Apalkov, J. Berashevich, K. Ziegler, and T. Chakraborty, "Properties of graphene: A theoretical perspective," *Adv Phys*, vol. 59, no. 4, pp. 261–482, 2010, doi: 10.1080/00018732.2010.487978.

[16] F. Paquin, J. Rivnay, A. Salleo, N. Stingelin, and C. Silva, "Multi-phase semicrystalline microstructures drive exciton dissociation in neat plastic semiconductors," *J. Mater. Chem. C*, vol. 3, pp. 10715–10722, 2015, doi: 10.1039/b000000x.

[17] F. Xiong, J. Zhang, Z. Zhu, X. Yuan, and S. Qin, "Ultrabroadband, More than One Order Absorption Enhancement in Graphene with Plasmonic Light Trapping," *Sci Rep*, vol. 5, no. October, pp. 1–8, 2015, doi: 10.1038/srep16998.

[18] M. Yankowitz *et al.*, "Emergence of superlattice Dirac points in graphene on hexagonal boron nitride," *Nat Phys*, vol. 8, no. 5, pp. 382–386, 2012, doi: 10.1038/nphys2272.

[19] A. L. Olatomiwa *et al.*, "Recent advances in density functional theory approach for optoelectronics properties of graphene," *Heliyon*, vol. 9, no. 3, p. e14279, Mar. 2023, doi: 10.1016/j.heliyon.2023.e14279.

[20] A. L. Olatomiwa *et al.*, "Recent advances in density functional theory approach for optoelectronics properties of graphene," *Heliyon*, vol. 9, no. 3, p. e14279, Mar. 2023, doi: 10.1016/j.heliyon.2023.e14279.

[21] F. Bonaccorso *et al.*, "Graphene, related two-dimensional crystals, and hybrid systems for energy conversion and storage," *Science (1979)*, vol. 347, no. 6217, 2015, doi: 10.1126/science.1246501.

[22] S. Khan, S. U. Zaman, R. Ahmad, N. Mehmood, M. Arif, and H. J. Kim, "Ab initio investigations of structural, elastic, electronic and optical properties of the fluoroperovskite TIXF3 (X=Ca, Cd, Hg, and Mg) compounds," *Mater Res Express*, vol. 6, no. 12, 2019, doi: 10.1088/2053-1591/ab5e37.

[23] O. Olaniyan, R. E. Maphasha, M. J. Madito, A. A. Khaleed, E. Igumbor, and N. Manyala, "A systematic study of the stability, electronic and optical properties of beryllium and nitrogen co-doped graphene," *Carbon N Y*, vol. 129, pp. 207–227, Apr. 2018, doi: 10.1016/j.carbon.2017.12.014.

[24] P. Nath, S. Chowdhury, D. Sanyal, and D. Jana, "Ab-initio calculation of electronic and optical properties of nitrogen and boron doped graphene nanosheet," *Carbon N Y*, vol. 73, pp. 275–282, Jul. 2014, doi: 10.1016/J.CARBON.2014.02.064.

[25] M. Gajdoš, K. Hummer, G. Kresse, J. Furthmüller, and F. Bechstedt, "Linear optical properties in the projector-augmented wave methodology," *Phys Rev B Condens Matter Mater Phys*, vol. 73, no. 4, 2006, doi: 10.1103/PhysRevB.73.045112.

[26] M. L. Ould NE, A. G. el hachimi, M. Boujnah, A. Benyoussef, and A. el Kenz, "Comparative study of electronic and optical properties of graphene and germanene: DFT study," *Optik (Stuttg)*, vol. 158, pp. 693–698, Apr. 2018, doi: 10.1016/j.ijleo.2017.12.089.

[27] G. Yang, L. Li, W. B. Lee, and M. C. Ng, "Structure of graphene and its disorders: a review," *Science and Technology of Advanced Materials*, vol. 19, no. 1. Taylor and Francis Ltd., pp. 613–648, Dec. 31, 2018. doi: 10.1080/14686996.2018.1494493.

[28] Z. Xu and M. J. Buehler, "Interface structure and mechanics between graphene and metal substrates: A first-principles study," *Journal of Physics Condensed Matter*, vol. 22, no. 48, Dec. 2010, doi: 10.1088/0953-8984/22/48/485301.

[29] N. N. Hieu *et al.*, "First-principles study of the structural and electronic properties of graphene/MoS2 interfaces," *J Appl Phys*, vol. 122, no. 10, Sep. 2017, doi: 10.1063/1.5001558.

[30] X. F. Fan, W. T. Zheng, V. Chihaia, Z. X. Shen, and J. L. Kuo, "Interaction between graphene and the surface of SiO 2," *Journal of Physics Condensed Matter*, vol. 24, no. 30, Aug. 2012, doi: 10.1088/0953-8984/24/30/305004.

[31] "Optoelectronic behavior of ZnS compound and its alloy_ A first principle approach _ Elsevier Enhanced Reader".

[32] K. S. Novoselov *et al.*, "Electronic properties of graphene," in *Physica Status Solidi (B) Basic Research*, Nov. 2007, pp. 4106–4111. doi: 10.1002/pssb.200776208.

[33] O. V. Sedelnikova, L. G. Bulusheva, and A. V. Okotrub, "Ab initio study of dielectric response of rippled graphene," *Journal of Chemical Physics*, vol. 134, no. 24, Jun. 2011, doi: 10.1063/1.3604818.

[34] A. L. Olatomiwa, T. Adam, S. C. B. Gopinath, S. Y. Kolawole, O. H. Olayinka, and U. Hashim, "Graphene synthesis, fabrication, characterization based on bottom-up and top-down approaches: An overview," *Journal of Semiconductors*, vol. 43, no. 6, p. 061101, Jun. 2022, doi: 10.1088/1674-4926/43/6/061101.

[35] M. Srivastava, A. Srivastava, and S. K. Pandey, "Suitability of graphene monolayer as sensor for carcinogenic heavy metals in water: A DFT investigation," *Appl Surf Sci*, vol. 517, p. 146021, Jul. 2020, doi: 10.1016/J.APSUSC.2020.146021.

[36] M. Houmad, H. Zaari, A. Benyoussef, A. el Kenz, and H. Ez-Zahraouy, "Optical conductivity enhancement and band gap opening with silicon doped graphene," *Carbon N Y*, vol. 94, pp. 1021–1027, Aug. 2015, doi: 10.1016/j.carbon.2015.07.033.

[37] S. K. Tiwari, S. Sahoo, N. Wang, and A. Huczko, "Graphene research and their outputs: Status and prospect," *Journal of Science: Advanced Materials and Devices*, vol. 5, no. 1, pp. 10–29, Mar. 2020, doi: 10.1016/J.JSAMD.2020.01.006.

[38] T. Ando, "The electronic properties of graphene and carbon nanotubes," *NPG ASIA MATERIALS | NPG Asia Mater*, vol. 1, no. 1, pp. 17–21, 2009, doi: 10.1038/10.1038/asiamat.2009.1.

[39] S. Khan, S. U. Zaman, R. Ahmad, N. Mehmood, M. Arif, and H. J. Kim, "Ab initio investigations of structural, elastic, electronic and optical properties of the fluoroperovskite TIXF3 (X=Ca, Cd, Hg, and Mg) compounds," *Mater Res Express*, vol. 6, no. 12, 2019, doi: 10.1088/2053-1591/ab5e37.

[40] M. H. Mohammed, "Controlling the electronic properties of the graphene nanoflakes by BN impurities," *Physica E Low Dimens Syst Nanostruct*, vol. 95, pp. 86–93, Jan. 2018, doi: 10.1016/J.PHYSE.2017.09.014.

[41] S. Y. Davydov, "On the specific features of the density of states of epitaxial graphene formed on metal and semiconductor substrates," *Semiconductors*, vol. 47, no. 1, pp. 95–104, 2013, doi: 10.1134/S1063782613010090.

[42] A. B. Ahmed, M. Said, and A. A. Sisa, "A QUANTUM ESPRESSO STUDY OF NITROGEN DOPED

GRAPHENE USING DENSITY FUNCTIONAL THEORY," *Bima Journal of Science and Technology*, vol. 5, no. 3, 2022.

[43] A. Bouhlal, A. Jellal, and N. M. Shah, "Zero-energy states in graphene quantum dot with wedge disclination."

[44] R. Sharma, S. Khan, V. Goyal, V. Sharma, and K. S. Sharma, "Investigation on effect of boron and nitrogen substitution on electronic structure of graphene," *FlatChem*, vol. 1, pp. 20–33, Jan. 2017, doi: 10.1016/J.FLATC.2016.10.001.

[45] J. D. ; Ortega-López and C. ; Espitia-Rico, "Citation: Morinson-Negrete," 2022, doi: 10.3390/ma15082731.

[46] L. Lu *et al.*, "Fano Resonance Ion Sensor Enabled by 2D Plasmonic Sub-Nanopores-Material," *IEEE Sens J*, vol. 21, no. 13, 2021, doi: 10.1109/JSEN.2021.3065409.

[47] S. Nigar, Z. Zhou, H. Wang, and M. Imtiaz, "Modulating the electronic and magnetic properties of graphene," 2017, doi: 10.1039/c7ra08917a.

[48] C. Yang *et al.*, "Metallic Graphene-Like VSe2 Ultrathin Nanosheets: Superior Potassium-Ion Storage and Their Working Mechanism," *Advanced Materials*, vol. 30, no. 27, Jul. 2018, doi: 10.1002/adma.201800036.

[49] P. Rani, G. S. Dubey, and V. K. Jindal, "DFT study of optical properties of pure and doped graphene," *Physica E Low Dimens Syst Nanostruct*, vol. 62, pp. 28–35, Aug. 2014, doi: 10.1016/J.PHYSE.2014.04.010.

[50] A. Ayatollahi, M. R. Roknabadi, M. Behdani, N. Shahtahmassebi, and B. Sanyal, "Adsorption characteristics of amino acids on graphene and germanene using dispersion-corrected density functional theory," *Physica E Low Dimens Syst Nanostruct*, vol. 127, p. 114498, Mar. 2021, doi: 10.1016/J.PHYSE.2020.114498.

[51] M. Goudarzi, S. S. Parhizgar, and J. Beheshtian, "Electronic and optical properties of vacancy and B, N, O and F doped graphene: DFT study," *Opto-Electronics Review*, vol. 27, no. 2, pp. 130–136, Jun. 2019, doi: 10.1016/j.opelre.2019.05.002.

[52] M. L. Ould NE, A. G. el hachimi, M. Boujnah, A. Benyoussef, and A. el Kenz, "Comparative study of electronic and optical properties of graphene and germanene: DFT study," *Optik (Stuttg)*, vol. 158, pp. 693–698, Apr. 2018, doi: 10.1016/j.ijleo.2017.12.089.

[53] A. Najim, O. Bajjou, M. Boulghallat, K. Rahmani, and L. Moulaoui, "DFT study on electronic and optical properties of graphene under an external electric field," *E3S Web of Conferences*, vol. 336, p. 00006, 2022, doi: 10.1051/e3sconf/202233600006.

[54] M. Rafique, Y. Shuai, and N. Hussain, "First-principles study on silicon atom doped monolayer graphene," *Physica E Low Dimens Syst Nanostruct*, vol. 95, pp. 94–101, Jan. 2018, doi: 10.1016/J.PHYSE.2017.09.012.

[55] O. Olaniyan, R. E. Maphasha, M. J. Madito, A. A. Khaleed, E. Igumbor, and N. Manyala, "A systematic study of the stability, electronic and optical properties of beryllium and nitrogen co-doped graphene," *Carbon N Y*, vol. 129, pp. 207–227, Apr. 2018, doi: 10.1016/j.carbon.2017.12.014.

[56] E. Pallecchi *et al.*, "High Electron Mobility in Epitaxial Graphene on 4H-SiC(0001) via post-growth annealing under hydrogen," 2014, doi: 10.1038/srep04558.

[57] F. Ostovari, M. Hasanpoori, M. Abbasnejad, and M. A. Salehi, "DFT calculations of graphene monolayer in presence of Fe dopant and vacancy," *Physica B Condens Matter*, vol. 541, pp. 6–13, Jul. 2018, doi: 10.1016/J.PHYSB.2018.04.023.

[58] X. S. Dai, T. Shen, and H. C. Liu, "DFT study on electronic and optical properties of graphene modified by phosphorus," *Mater Res Express*, vol. 6, no. 8, Jun. 2019, doi: 10.1088/2053-1591/ab29bc.

[59] P. Nath, S. Chowdhury, D. Sanyal, and D. Jana, "Ab-initio calculation of electronic and optical properties of nitrogen and boron doped graphene nanosheet," *Carbon N Y*, vol. 73, pp. 275–282, Jul. 2014, doi: 10.1016/J.CARBON.2014.02.064.

[60] P. E. Batson' and J. Silcox, "Experimental energy-loss function, Im[-1/e(q, co)], for aluminum," 1983.

[61] S. Cheon and K. D. Kihm, "Handbook of Graphene," 2019.

[62] M. Houmad, H. Zaari, A. Benyoussef, A. El Kenz, and H. Ez-Zahraouy, "Optical conductivity enhancement and band gap opening with silicon doped graphene," *Carbon N Y*, vol. 94, pp. 1021–1027, Nov. 2015, doi: 10.1016/J.CARBON.2015.07.033.

[63] R. Sharma, S. Khan, V. Goyal, V. Sharma, and K. S. Sharma, "Investigation on effect of boron and nitrogen substitution on electronic structure of graphene," *FlatChem*, vol. 1, pp. 20–33, Jan. 2017, doi: 10.1016/j.flatc.2016.10.001.

[64] P. Rani and V. K. Jindal, "Designing band gap of graphene by B and N dopant atoms," *RSC Adv*, vol. 3, no. 3, pp. 802–812, Jan. 2013, doi: 10.1039/c2ra22664b.

[65] O. Olaniyan *et al.*, "Exploring the stability and electronic structure of beryllium and sulphur co-doped graphene: A first principles study," *RSC Adv*, vol. 6, no. 91, pp. 88392–88402, 2016, doi: 10.1039/c6ra17640b.

[66] P. Rani, G. S. Dubey, and V. K. Jindal, "DFT study of optical properties of pure and doped graphene," *Physica E Low Dimens Syst Nanostruct*, vol. 62, pp. 28–35, Aug. 2014, doi: 10.1016/J.PHYSE.2014.04.010.

[67] M. Houmad, H. Zaari, A. Benyoussef, A. el Kenz, and H. Ez-Zahraouy, "Optical conductivity enhancement and band gap opening with silicon doped graphene,"

Carbon N Y, vol. 94, pp. 1021–1027, Nov. 2015, doi: 10.1016/J.CARBON.2015.07.033.

[68] M. Rafique, Y. Shuai, and N. Hussain, "First-principles study on silicon atom doped monolayer graphene," *Physica E Low Dimens Syst Nanostruct*, vol. 95, pp. 94–101, Jan. 2018, doi: 10.1016/j.physe.2017.09.012.

Table 1. Pure graphene's predicted structural and electronic properties in recent and earlier investigations

Structural Properties				
	Total Energy (eV)	**Optimized Volume (a.u^3)**	**Bond length (Å)**	**Reference**
Current Study	-4147.42	355.97	1.42	NA
Previous Study	-2073.10	357.81	1.42	[63], [64]
Electronic Properties				
	Band Gap (eV)	**The density of State (eV)**		**References**
Current Study	0	0		NA
Previous Study	0	0		[26], [63], [65]

Table 2. The calculated magnetic moment (μ_B) for Pristine graphene

Spin Magnetic Moment in a cell	**Magnetic Moment in interstitial**	**Magnetic Moment in Sphere 1**	**Magnetic Moment in Sphere 2**
-0.07522	-0.00307	-0.00319	-0.08775

Table 3. The major peaks of Pure Graphene's optical properties in current and previous investigations

Peaks of the Optical Properties of The Current Study						
	Absorption Coefficient (eV)	**Refractive Index (eV)**	**Reflectivity (eV)**	**Optical Conductivity (eV)**	**Optical Transparency (eV)**	**References**

Parallel Polarization	4.2 & 13.8	4.0 & 11.8	4.2 & 13.8	4.2 & 13.8	8.6 - 10.4	NA
Perpendicular Polarization	12.0	10.4	13.8	10.6	NA	NA
Peaks of the Optical Properties of Previous Study						
	Absorption Coefficient (eV)	**Refractive Index (eV)**	**Reflectivity (eV)**	**Optical Conductivity (eV)**	**Optical Transparency (eV)**	**References**
Parallel Polarization	4.0 & 14.0	4.0 & 11.4	4.3 & 14.0	3.78	7.5 – 10.0	[23], [66], [67]
Perpendicular Polarization	14.0	10.89	14.9, 14.0	NA	NA	[68]

Table 4 The behavior of the atomic, electronic, and optical properties of pure graphene

Atomic Structure	**Electronic Properties**	**Absorption Spectra**	**Refractivity**	**Optical Conductivity**
Hexagonal lattice structure	Zero band gap	Ultraviolet ranges (4.2eV ≈ 311nm)	Ultraviolet ranges (4.2eV ≈311nm)	Metallic Behaviour

Figure 1. The optimized pure graphene Supercell structure

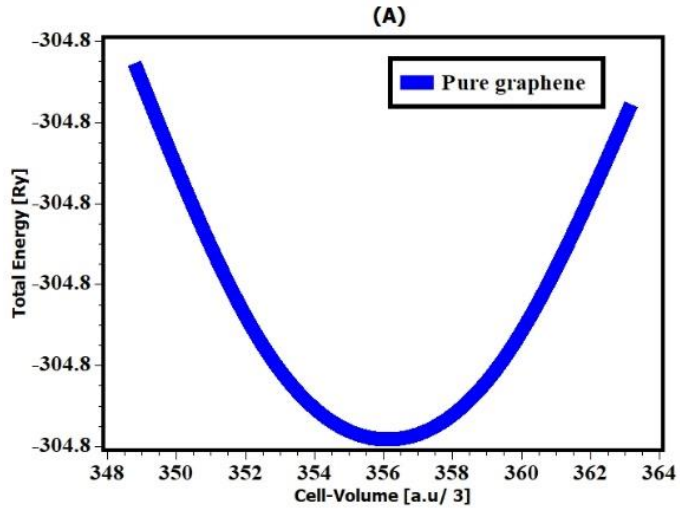

Figure 2. Pure graphene's total energy per atom as a function of volume

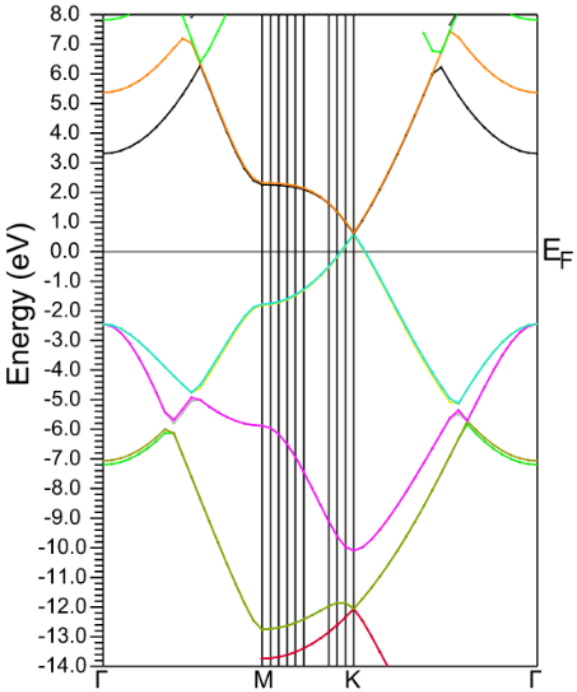

Figure 3. Band structure for Pristine Graphene based on PBE exchange-correlation functional

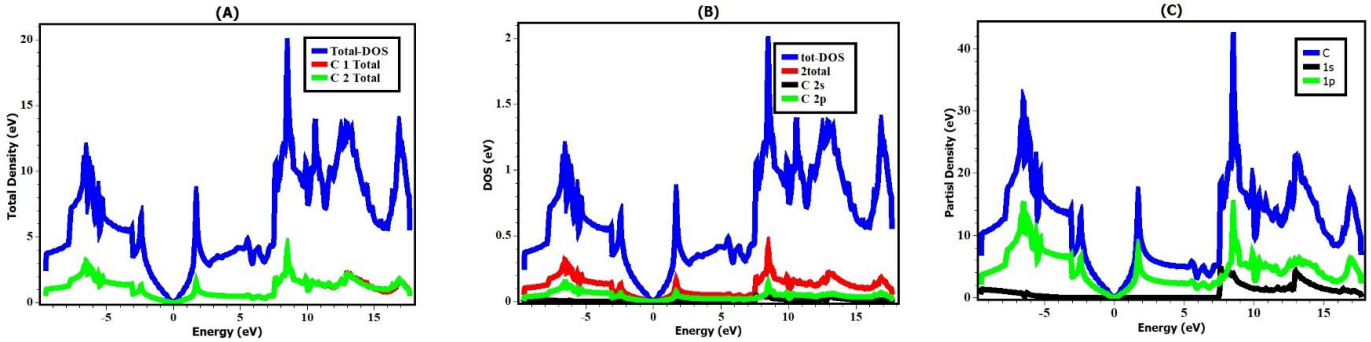

Figure 4. The calculated (a) Total density of State (b) Total and Partial Density of State (c) Partial density of State for Pristine graphene

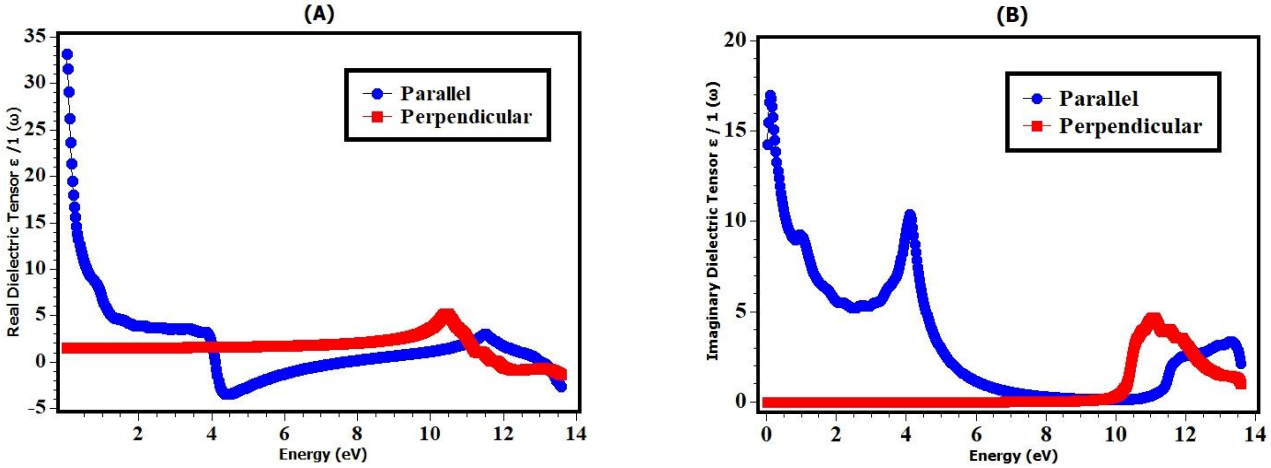

Figure 5. The calculated (a) real ε_1 and (b) imaginary ε_2 part of the dielectric function of pristine graphene

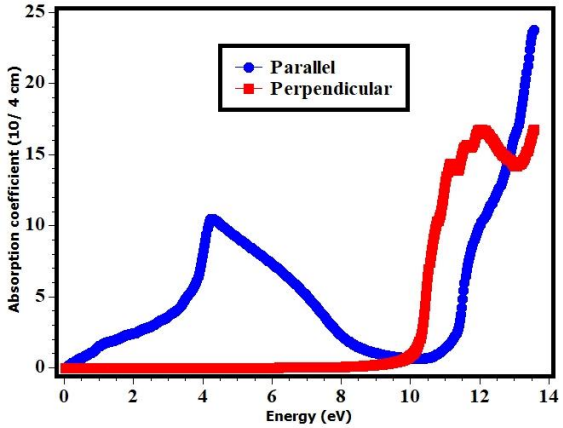

Figure 6. The calculated absorption coefficient of pristine graphene as a function of incident light in the parallel and perpendicular polarization

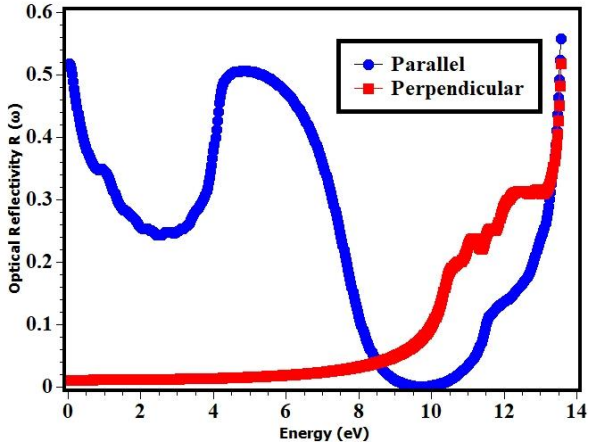

Figure 7. The reflectivity of pristine graphene with photon energy and wavelength

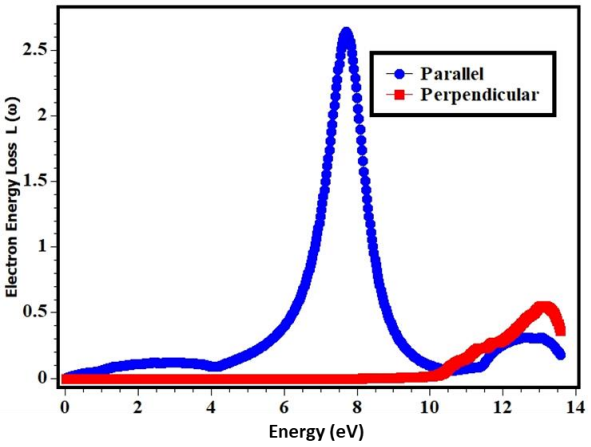

Figure 8. The calculated energy loss function of pristine graphene

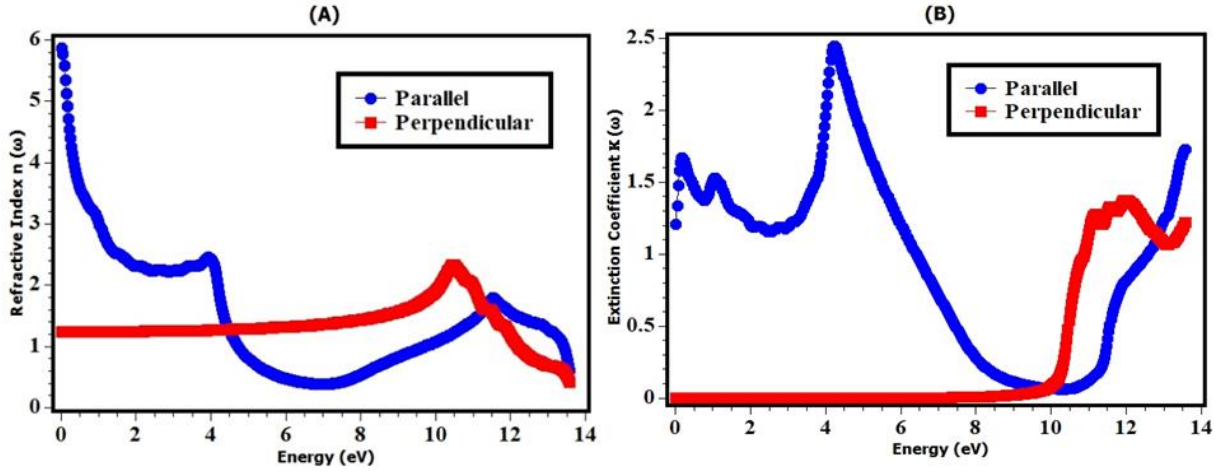

Figure 9. The calculated (a) refractive index $n\ (\omega)$ and (b) extinction coefficient $\kappa(\omega)$ of pure graphene

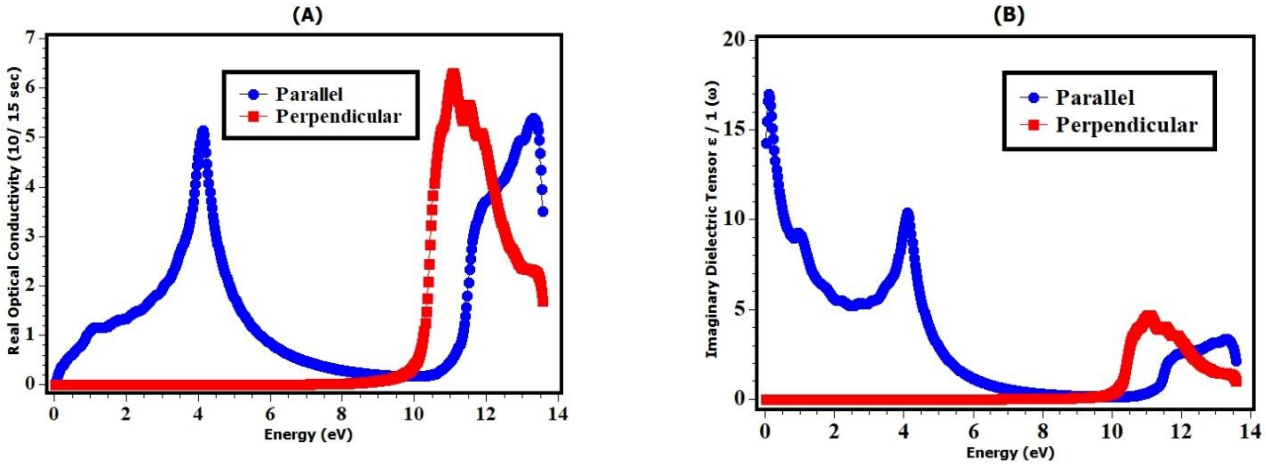

Figure 10. The calculated (a) real and (b) imaginary optical conductivity of pristine graphene